Monitoring Carbon Dioxide Sequestration Using Electrical Resistance Tomography (ERT): Sensitivity Studies

Robin L. Newmark (newmark@llnl.gov, 925-423-3644)
Abelardo L. Ramirez (ramirez3@llnl.gov; 925-422-6909)
William D. Daily (daily1@llnl.gov; 925-422-8623)

Lawrence Livermore National Laboratory
P.O. Box 808
Livermore, Ca. 94550

Abstract

If geologic formations are used to sequester carbon dioxide (CO_2), monitoring the CO_2 injection will be required to confirm the performance of the reservoir system, assess leaks and flow paths, and understand the geophysical and geochemical interactions between the CO_2 and the geologic minerals and fluids. Electrical methods are well suited for monitoring processes involving fluids, as electrical properties are sensitive to the presence and nature of the formation fluids. High resolution tomographs of electrical properties are now possible using a 3D technique called electrical resistance tomography (ERT). Surveys are commonly conducted utilizing vertical arrays of point electrodes in a cross-well configuration. Recent field results obtained using steel well casings as electrodes are promising. When 3D ERT imaging can be performed using existing well casings as long electrodes, the need for additional drilling of observation wells is minimized.

Using a model patterned after an oil field undergoing CO_2 flood, forward and inverse simulations of ERT surveys have been run to test the sensitivity of the method to changes resulting from CO_2 migration. Factors considered include resistivity contrast, anomaly proximity to electrodes, anomaly size and shape, measurement noise, and the electrode configuration used to perform the measurements. Field data suggest that CO_2 migration changes the resistivity of a layer, producing an anomalous region. In our numerical study, the anomalous region's resistivity ranges from 0.2 to 10 times that of the initial value. Its geometry ranges from a thin, horizontal finger to a planar, horizontal mass having vertical protrusions simulating leakage of CO_2 through caprock. Results of simulations run assuming that well casings are used as long electrodes or with arrays of point electrodes (simulating high resolution surveys) show useful information for even the narrowest simulated CO_2 fingers.

Introduction

If geologic formations are to be used to sequester CO_2, it will be necessary to monitor the process. Monitoring is necessary to confirm the reservoir performance, assess leaks and flow paths and gain understanding into interactions between CO_2, the formation and

formation fluids. Remote methods are preferred, both to minimize disruption and to reduce costs.

Electrical methods are particularly well suited for monitoring processes involving fluids. The electrical properties of geologic systems depend on many of the same factors relevant to CO_2 sequestration. The electrical resistivity and impedance of rocks and soils depend on: water saturation, the amount and type of ions in the water, pH, cation exchange capacity of the minerals, and on temperature. As a result of these dependencies, high resolution tomographs of electrical properties have been used with success for both site characterization and to monitor subsurface migration of various fluids such as subsurface steam floods, underground tank leaks, water infiltration events, and contaminant movement (Daily et al., 1992; Daily et al., 1998; LaBrecque et al., 1998, Newmark *et al*., 1994, Newmark *et al.*, 1998, Ramirez *et al*., 1993; Ramirez *et al*., 1996). Electrical imaging techniques have also been used successfully to monitor the integrity of subsurface barriers (Daily and Ramirez, 2000). High resolution field surveys such as these are typically conducted using subsurface "point" electrode arrays in a cross-well configuration. By "point" we mean that the electrode size is much smaller than the distance separating adjacent electrodes.

An exciting new development in electrical imaging methodology is the potential to use the existing subsurface infrastructure to image the reservoir. Since metallic casings are electrically conductive, they can be used as long electrodes, thus permitting the same infrastructure to have a dual operational and monitoring role. In recent field tests using abandoned steel casings in an oil field undergoing steam flood, mapped changes in the electrical properties were found that were consistent with production events (Newmark et al., 1999, 2000). If such imaging can be performed using operational casings as electrodes, this provides a nearly noninvasive method for monitoring and process control, essential for safe and effective carbon management in the future.

ERT imaging using existing subsurface infrastructure has many advantages. The objective is to produce time dependent maps of changes in formation resistivity caused by CO_2 injection and migration. Using the existing subsurface infrastructure would be minimally to non-invasive, with no disruption to injection/production activities, and requiring no additional drilling. Vertical wells alone can provide information regarding the lateral changes in a field. If horizontal wells are available, some vertical resolution may be provided as well. Using existing casings for data acquisition results in lower manpower requirements because the measurements can be made in an automated, remote fashion; these capabilities translate into lower costs. The ability to conduct surveys at any time, without disrupting operations, is highly desirable. Using the existing field infrastructure provides a stable base against which subsequent changes in the field can be readily measured. This is in contrast with conventional surveys, which require instrument locations to be resurveyed as part of each fielding. In addition to providing insight into injection/sequestration performance over time, such surveys would provide a context for decisions regarding the deployment of more focused (and more expensive) survey methods such as high resolution 3D seismic.

Approach

We have conducted a series of sensitivity studies to map out the ERT performance envelope using realistic CO_2 flood model scenarios. Using published field data and unpublished information obtained through communication with industry collaborators, we developed a set of target scenarios indicative of realistic CO_2 injection projects. Numerical simulations were conducted to investigate the range of conditions and measurement configurations under which ERT methods may be used to monitor the geophysical changes resulting from CO_2 injection and migration.

Site Model:

The model used was patterned after a pilot CO_2 flood conducted in an operating oil field. The test is known as the Maljamar pilot, and was conducted in Lea County, New Mexico during the mid 1980s (Albright, 1984). The flooded layers consisted of dolomitic sands and dolomites, located at depths of 1130 and 1230 m. The pilot flood used a 5 acre, inverted 5 spot arrangement for the injection/production wells (the center well was used for injection).Two observation wells provided access to the flood zones and were used to conduct a suite of well logs that included induction logs. The induction logs sampled the electrical properties of the layers before, during and after the CO_2 flood. They showed that the resistivity of the layers increased by about a factor of 5 during the CO_2 flood.

Numerical Model:

We constructed a numerical model that exhibits electrical properties similar to those of the Maljamar pilot. In our model, we assume that CO_2 is injected into a single 14 m thick layer located at depth. The pre-flood resistivity of the layer is set to 10ohm-m. The numerical modeling varied a number of factors known to affect the sensitivity and resolution of ERT. These factors include resistivity contrast, the anomaly's size, shape and proximity to electrodes, measurement error, and electrode deployment. A 9 spot, 20 acre pattern of wells was selected to simulate realistic oil-field scales. The wells surround a block that is 285 m x 285 m (horizontally), with well spacing equal to 142 m. The model considers three electrode deployment scenarios:

a) 9 vertical wells, with 10 "point" electrodes in each
b) 9 vertical steel cased wells used as long electrodes
c) 9 vertical, 6 horizontal casings used as long electrodes.

Although the "point" electrode deployment is typically considered to provide the highest resolution, the relatively large spacing between electrodes (28.4 m vertically, 142 m laterally) makes this measurement configuration quite coarse relative to the more common environmental applications of the method. However, this larger spacing is more representative of the oil field scale, and could be considered a worst-case scenario for "point" electrode deployment in terms of resolution.

Figure 1 depicts these deployment scenarios and the resistivity model corresponding to the pre-flood or baseline case. The pre-flood resistivity of the layers was set to 10 ohm-m

surrounded by a 100 ohm-m background. To simulate the effects of CO_2 , the electrical properties of the center layer in Figure 1 were changed as follows: flood layer, initially at 10 ohm-m, changed to 100, 50, 20, 15, 13, 11, or 2 ohm-m. These resistivity values translate into changes ranging from +900% to –80%. Note that this range includes the +400% change observed during the Maljamar pilot as well as smaller changes. The smaller changes allow us to study the performance of the technique at the lower limits of sensitivity.

We tested 6 anomaly shapes, designed to model expected reservoir scenarios. These included:

1) 3 horizontal tabular bodies, positioned at different locations relative to the center well in the 9 spot pattern,
2) a narrow "finger" anomaly simulating a preferential flow path within the layer, and,
3) vertical penetrations originating from an initial horizontal tabular body, simulating a vertical breach of the caprock above the reservoir unit.

For the models assuming that steel casings are used as very long electrodes, the casing resistivity is assumed to be 10^{-5} ohm-m. Thus, the contrast between casings and the surrounding rock is 6 or 7 orders of magnitude.

Using this suite of models, the forward problem was solved using a 3D, finite difference technique described by LaBrecque and Morelli (1996). The calculated data was corrupted by adding to it noise from a uniformly random distribution (+/- 2%). The inverse problem was then solved using the corrupted data. The 3D inverse algorithm used is described by LaBrecque and Morelli (1996). The inverse problem allows for higher model roughness in the vertical direction than in the horizontal directions.

Results

Point Electrode Scenario:

Figure 2 shows some of the results obtained for two electrode deployment scenarios: "point electrode" arrays and vertical casings used as long electrodes. The top row of images (row "A") shows the outline of the anomalies assumed. Note that the L1, L2 and L6 models consist of tabular bodies located at various positions within the flood layer. Model L3 simulates a "finger-like" preferential flow path between the center of the pattern and one of its sides. Models L4 and L5 consist of a tabular body that connects to a vertical pillar; the pillar simulates a breach of the caprock by the CO_2 flood. Its resistivity contrast is preserved in the caprock layer. In L4, the closest distance between the pillar and the nearest electrode is about 80 m. In L5, the pillar is located with 15 m of the center electrode array. This means that the pillar in model L5 should be easier to detect and resolve. The L6 model is identical to L4 and L5 but does not have a pillar associated with it.

Rows “B” and “C” show results for the “point” electrode simulations. Note that the results in Rows “B” and “C” form the two end members of the range of resistivity contrasts considered by this study. Row “B” shows the results obtained when the magnitude of the change in the model is +900% (flood layer, initially at 10 ohm-m, changed to 100 ohm-m). The color bar at the bottom-left and bottom-right of the figure shows the mapping between the colors and percent resistivity change; the white bar located within the color bar indicates the range of values that have been made transparent in order to be able to look inside the block. The L1, L2 and L3 results in Row “B” show a coarse resemblance to the models in Row “A”. In general, the tomograph anomalies are wider and thicker than the models. This is due to the smoothness-constrained inversion approach that finds solutions that have maximum smoothness. This approach causes the anomaly volume to be exaggerated and the magnitude of the resistivity change to be under-predicted. Later in the paper, this aspect will be discussed in more detail. These results suggest that it may be possible to produce useful images of lateral distribution of the CO_2 flood using “point” electrodes.

The L4 and L5 results in Row “B” are a poor match to the corresponding models in Row “A”. There is relatively little difference between the L4, L5 and L6 results. Although the horizontal tabular body is relatively well resolved, the pillars are barely noticeable. These results suggest that it may be hard to detect breaches of the caprock by the CO_2 flood when the resistivity increases, at least with such large electrode separations.

Row “C” shows the results obtained in a case where the resistivity decreases 80% (flood layer, initially at 10 ohm-m, changed to 2 ohm-m). Such a change could be caused by brine injection. In general, the shapes and sizes of the anomalies in Rows “B” and “C” are similar for models L1, L2 and L3. Noticeable differences are present for anomalies L4 and L5. The Row “C” anomalies are noticeably thicker than the corresponding ones in Row “B”. The points of maximum thickness approximately coincide with the location of the pillars, although the shapes of the pillars are poorly resolved. The L4 and L5 anomalies are also significantly different from the L6 anomaly in Row “C”. Given the electrode spacing assumed here, this means that it may be possible to detect (but not resolve) a caprock breach when the CO_2 flood causes the resistivity to decrease.

Vertical Casings As Long Electrodes:

The potential field created by vertical long electrodes has a vertical gradient that is near zero. Consequently, it not possible to locate the vertical position or extent of the anomalies, but it is possible to coarsely locate their horizontal position and extent. Row “D” in Figure 2 shows the results obtained when 9 vertical steel casings are used as very long electrodes (length = 1438 m). We only show a horizontal slice through the image because there is no variability in the vertical direction. The lateral extent of all anomalies except L3 is mapped reasonably well. Note that the images corresponding to the L1 and L2 models show anomalies in the correct horizontal position, and approximately correct lateral extent. Similar observations can be made about the L4, L5, and L6 anomalies; due to the lack of vertical resolution, the pillar portion of the anomalies is not resolved, although the magnitude of the change is more pronounced in the cases where the pillars

exist. Only a piece of the L3 “finger” anomaly can be seen. This anomaly is significantly smaller in volume than the other anomalies, and consequently it is harder to detect and resolve.

While measurement configurations using metallic casings as long electrodes were included in these simulations, it is important to note that operational changes are required to permit such measurements to be made in the field. It will be necessary to electrically de-couple the surface piping from the subsurface casing. This can be readily accomplished by installing an electrically insulating sub or spacer at the wellhead. Modifications to the normal data acquisition systems will also be necessary in order to handle the high amperage needed to achieve acceptable signal to noise ratio in the field.

Vertical And Horizontal Casings As Long Electrodes:

Some of the reservoirs that may be used for CO_2 sequestration contain horizontal steel cased wells, in addition to the more common vertical wells. When horizontal wells are available, they might be used as long electrodes together with the vertical steel-cased wells. This combination may provide the capability to coarsely resolve targets vertically and horizontally.

Figure 3 compares the results obtained using the three electrode deployment scenarios examined in this study. In this case, we compare the results for the L1 model when the center layer resistivity changes from 10 to 50 ohm-m. The upper-left image (A) shows the true model. The upper right image (B) shows the results obtained when the point electrode arrays are used. Image C, on the lower left of the figure, shows the results obtained when 9 vertical steel-cased wells are used. Image D, on the lower right of the figure, shows the results obtained when 9 vertical and 6 horizontal steel-cased wells are used. The color bar on the left applies to images A and B while the one on the right applies to images C and D. Different transparency windows make up the difference between color bars.

Image C clearly shows that the vertical casing results can only be used to map the lateral position and extent of the target. Image D shows that, when horizontal well data is added, the vertical position and extent of the target can be recovered. A comparison of images B and D suggests that the results are similar. However, the thickness of the anomaly is more exaggerated in D and the resistivity change in D is weaker than in C. This is the reason why two different color bars are used to display the results.

For the case of the “finger” model (L3 model in Figure 2), the difference between the “point” electrode and long electrode results are more substantial. In this case, the “point” electrode results are clearly superior.

In summary, coarse lateral resolution should be possible when using vertical steel casings as long electrodes. When both vertical and horizontal steel casings are used, coarse lateral and vertical resolution may be obtained. This means that it may be possible to map changes associated with a CO_2 flood using long electrodes. This approach helps reduce

costs by reducing or eliminating the need for dedicated observation wells, and by minimizing disruption to reservoir operations in order to make measurements from within injector/producer wells.

Quantitative Analysis Of Image Quality: Point Electrode Results

The previous discussion has focused on qualitative analysis of the images. A quantitative analysis of the method's reliability is also important, because in many applications we wish to convert the resistivity values to other parameters such as water saturation or the resistivity of the pore fluid. To estimate the reliability of such conversions, it is necessary to characterize the reliability of the resistivity values in the images. Here, we concentrate the analysis on "point" electrode results.

Voxel position:

Figure 4 can be used to evaluate the influence that voxel position has on the magnitude of the resistivity change recovered by the tomographs. Here we consider a centered tabular anomaly that is relatively easy to resolve (model L1 in Figure 2), and a narrow "finger" anomaly (model L3 in Figure 2) which presents a more difficult challenge. The graphs on the left side of Figure 4 compare the "true" percent resistivity change (in the model) to the recovered percent resistivity change in the tomograph for the various magnitudes of resistivity change considered. The top graph corresponds to the tabular anomaly and the bottom to the "finger" anomaly. Horizontal slices through the 3D mesh are shown on the right hand side of the figure. These slices show the location of the anomalies in the mesh (red color), the location of the point electrode arrays (white circles), and the location of the voxels to be examined. The symbols on the graphs (square, triangle, and diamond) also appear in the mesh slices to indicate the correspondence between graph values and mesh location.

We first consider the tabular anomaly in Figure 4. The corresponding graph shows a line that indicates "perfect" matching between model and tomograph values. The rose-colored square symbols come closest to the line. This symbol represents a voxel within the region occupied by the anomaly and near central electrode array. The green-colored triangle identifies a voxel at the edge of the anomaly and farther removed from the electrode arrays. For this voxel, the values in the tomograph are much smaller than values in the model. There are two causes for this behavior. One is that the method's sensitivity to any give voxel value depends on the distance between the voxel and the electrode arrays. A second reason is that the inverse algorithm makes use of a smoothness-constrained least-squares technique that searches for models having minimal contrast between adjacent voxels. This technique "smears" the resistivity value in a given voxel to adjacent voxels. Thus, the smoothness-constraint tends to produce models which tend to under-predict resistivity values in voxels that are removed from the electrodes. The last voxel, the blue diamond, is outside the anomalous region and nearly equidistant from the electrode arrays. It shows very little resistivity change, as expected.

Now consider the results corresponding to the "finger" anomaly in Figure 4. Again we can see that the voxel closest to an electrode array (rose-colored square), comes closest to the "perfect match line". The voxel identified by the blue diamond is within the anomaly,

but farther removed from the electrode arrays, and thus under-predicts the apparent resistivity change to a larger extent. These observations are similar to those for the tabular anomaly. However, the under-prediction of resistivity values is more pronounced for the "finger" anomaly. This is probably due to the fact that it has a significantly smaller volume than the tabular anomaly.

***Measurement error**:*
We also examined the effects of measurement error on the reliability of the tomographs. Specifically, we evaluated the influence that measurement error magnitude has on the reliability of relatively small resistivity changes. We also considered the effects that noise correlated in time may have on resistivity change images. Uniformly distributed random number sets were used to corrupt the data. For some of the simulations, the "pre-flood" and "during flood" data sets were corrupted using different sets of random numbers. For other simulations, the "pre-flood" and "during flood" data sets were corrupted using the same random number set in order to simulate noise that is correlated in time.

We first discuss the influence that noise magnitude may have on the images. Figure 5 shows the results of simulations where different levels of noise were added to the data. We chose the "finger" anomaly, because it is the smallest anomaly and the most difficult one to detect. Simulations for the other anomaly geometries showed better results overall. The top row shows the results when 2% noise was added to the data and the inversion algorithm assumed that the standard deviation of the data was 2%. In our experience, 2% measurement errors are typical of most ERT surveys. Note that, for the case of 30% change in model resistivity, pieces of the "finger" anomaly can be seen. However, other regions of the image show changes that are just as significant. When the resistivity change is only 10%, the finger anomaly is unobservable.

The bottom row of images in Figure 5 shows the results when 0.2% was added to the data and the inversion algorithm assumed that the standard deviation of the data was 0.2%. This level of noise is unusually low, but achievable in the field by such means as stacking the data for longer periods of time, increasing the received voltages by increasing the transmitted voltage, and using non-polarizing electrodes. The bottom row of images in Figure 5 shows that the finger anomaly can be resolved for both magnitudes of resistivity change. These results suggest that measurement error can have a significant influence in situations where the magnitude of change is small and the anomaly is relatively small in volume. For situations where the magnitude of change and the anomaly size are relatively large, the magnitude of the measurement error had an insignificant effect on the anomalies. Our analysis also suggests that very similar tomographs are obtained regardless of whether the noise is correlated in time or not.

When different 2% uniformly distributed random noise sets were added to simulations where the change in resistivity was 400%, we made the following observations. The resistivity change tomographs show that voxels with the smallest changes had differences as much as 10% caused by differences in the measurement error. By contrast, the differences were found to be about 2% for voxels with the largest percent resistivity changes. This means that voxels exhibiting large resistivity changes are relatively

unaffected by measurement error, and voxels exhibiting small resistivity changes can be significantly affected.

Volume estimates:
ERT tomographs may be used to estimate the reservoir volume penetrated by the liquid CO_2, and to estimate CO_2 content in the various regions of the reservoir. This will require quantitative analyses, and we have analyzed some of our results with these applications in mind. In our analysis, we count the number of voxels in the tomograph that change above some prescribed threshold; the threshold is based on the measurement error analysis discussed previously. All voxels that show larger changes than the threshold are assumed to be part of the tomograph anomaly. We then divide the number of voxels in the tomograph by the number of voxels in the model to compare the anomaly volumes in the tomograph and in the model. Depending on the threshold value, this might be expected to produce a minimum volume. However, this effect is offset by the smoothing constraint, which acts to enlarge the anomalous area in the tomograms.

Figure 6 helps to illustrate the results of this analysis. The threshold assumed for the results shown was 20%. The top graph shows the volume ratios obtained as function of anomaly contrast and as function of model. Volume ratios with a value of 1.0 indicate that the volume estimate based on the tomograph is in perfect agreement with the model's volume. Values greater than 1.0 indicate that the anomaly in the tomograph occupies a larger volume than the anomaly in the model. Note that most of the volume ratios shown are greater than 1.0. Also note that the volume ratios increase as the contrast between the anomaly and the background increases; the largest ratios are observed when the resistivity change is +900%. The differences between the models is relatively small, and no particular model seems be particularly prone to over-prediction. We suggest that volume over-prediction is primarily due to the smoothness-constraint used by the inversion algorithm.

We also calculated the average resistivity of the anomalies in the tomograph and in the model. The bottom graph in Figure 6 compares the average tomograph resistivity of the voxels within the anomaly volume to the corresponding voxel resistivity value in the model. Note that the change in resistivity for an individual voxel is identical to a change in resistance. As before, values greater than 1.0 indicate that the average resistivity value for the tomograph anomaly is larger than the value in the model. The graph shows that all values are below 1.0, and that the ratio gets smaller with increasing anomaly contrast. We believe that the under-prediction of resistivity change is a second manifestation of the effects of the smoothness constraint.

A comparison of the two graphs in Figure 6 indicates that there is a tendency to over-predict volume and under-predict resistance change, and that these two effects are roughly inversely proportional. Based on this observation, we suggest that the algorithm finds anomalies that are electrically equivalent to the ones in the models, i.e., the change in resistance to current flow is approximately the same for the tomograph and model anomalies. But in doing so, the algorithm significantly distorts the anomaly and

corresponding resistivity values. We believe that these distortions can be explained on the basis of the smoothness constraint.

Conclusions

The results of our numerical simulations increase our confidence that the ERT method can provide useful information to operators and managers controlling CO_2 field operations regarding the progress and behavior of the CO_2 flood. In practice, ERT surveys would be conducted to produce time dependent maps of changes in formation resistivity caused by CO_2 injection and migration. This study quantifies the effects of a variety of factors that affect the resolution and accuracy of the ERT method, under realistic conditions of scale, contrast and measurement error. Information such as the shape, location, and lateral extent of the flood can be deduced. If point electrode arrays or horizontal wells are available, information regarding the vertical extent may also be deduced.

The following conclusions can be made based on this study. These conclusions will apply to problems of scale and contrast similar to those assumed here.

1) Of the electrode deployment scenarios considered, the "point" electrode approach offers the highest sensitivity to the changes caused by the CO_2 flood. This approach requires observation wells that contain electrodes. For even the most difficult anomaly shape, with typical measurement errors (approximately 2%), anomalies which cause resistivity changes on the order of 30% or larger can be detected and resolved reliably. When unusually low measurement errors (0.2%) are possible, resistivity changes as low as 10% can be reliably detected and resolved.
2) Vertical and horizontal steel casings can be used together as long electrodes to coarsely resolve vertically and horizontally the effects of a CO_2 flood. This approach does not require that observation wells be available. When only vertical steel casings are used as long electrodes, the shape of the anomaly can be resolved laterally but not vertically. Hardware changes are required to use steel casings as long electrodes.
3) The tomographs tend to exaggerate the volume of the anomalies and under-predict the magnitude of the changes in resistivity. These effects are largely independent of measurement error and strongly dependent on the regularization (smoothing approach) used by the inverse algorithm. The inverse algorithm tends to "smear" the resistivity values from any given voxel to adjacent voxels, thereby exaggerating the volume and under-predicting the resistivity.
4) The easiest anomalies to resolve are those located near the center of the 9 spot pattern considered, and those having the largest volume and contrast. The hardest anomalies to resolve are "finger" anomalies of low volume and contrast. Over the range of contrast considered, conductive and resistive anomalies can be resolved equally well.
5) CO_2 breaches of the caprock may be hard to resolve. These breaches may be coarsely resolved when the breach occurs close to a "point" electrode array. Note that, in this study, the electrode spacing is relatively large compared to the features of interest. If

the distances between electrode arrays (or individual electrodes in the arrays) are reduced, the ability to resolve a breach can be improved significantly.

Future work

A field test is being designed to demonstrate the ERT method in an active field undergoing CO_2 flood. Technical challenges include electrically decoupling surface piping from well casings, using insulating subs at the wellhead.

Acknowledgements

We gratefully acknowledge the support of DOE's Office of Basic Energy Sciences. This work was performed under the auspices of the U.S. Department of Energy by University of California Lawrence Livermore National Laboratory under contract No. W-7405-Eng-48.

References

Albright, J. C., 1984. Use of well logs to characterize fluid flow in the Maljamar CO_2 Pilot, Society of Petroleum Engineers (SPE) 59th Annual Technical Conference and Exhibition, Houston Texas, September 16-19, *SPE 1342*, 8 pp.

Daily, W., A. Ramirez, D. LaBrecque and J. Nitao, 1992. Electrical Resistivity Tomography of Vadose Water Movement, *Water Resources Research*, v. 28, no. 5, 1429-1442.

Daily, W. D., A. Ramirez and R. Johnson, 1998, Electrical impedance tomography of a perchloroethelyne release, *J. Envir. and Eng. Geophysics*, vol. 2, No. 3, pp. 189-201.

Daily, W. and A. Ramirez, 2000, Electrical imaging of engineered hydraulic barriers, *Geophysics*, vol. 65, no. 1, pp. 83-94.

LaBrecque, D.J, J. Bennett, G. Heath, S. Schima, and H. Sowers, 1998. Electrical resistivity tomography monitoring for process control in environmental remediation, Symposium on the Application of Geophysics to Engineering and Environmental Problems (SAGEEP) '98, Chicago, Illinois, March 22-26, 613-622.

LaBrecque, D. and G. Morelli, 1996. 3D Electrical Resistivity Tomography for Environmental Monitoring, Proceedings of the Symposium of the Application of Geophysics to Engineering and Environmental Problems, SAGEEP 1996, April 28-May 2, Keystone CO, pages 723-732.

Newmark, R.L., S. Boyd, W. Daily, R. Goldman, R. Hunter, D. Kayes, K. Kenneally, A. Ramirez, K. Udell, and M. Wilt, 1994. Using geophysical techniques to control in situ thermal remediation, Symposium on the Application of Geophysics to Engineering and Environmental Problems (SAGEEP) '94, Boston, Ma., March 27-31, 195-211.

Newmark, R.L., W.D. Daily, K.R. Kyle and A. L. Ramirez, 1998. Monitoring DNAPL pumping using integrated geophysical techniques, *Journal of Environmental and Engineering Geophysics*, v. 3, no.1, 7-14.

Newmark, R.L., W. Daily, A. Ramirez, 1999. Electrical resistance tomography using steel cased boreholes as electrodes (UCRL-JC-131572), Society of Exploration Geophysicists 1999 SEG Annual Meeting, November, 1999.

Newmark, R.L., W. Daily, A. Ramirez, 2000. Electrically imaging EOR stimulation using steel-cased boreholes, (SPE 62567), SPE/AAPG Western Regional Meeting, June 19-23, Long Beach, California.

Ramirez, A., W. Daily, A. Binley, D. LaBrecque, and D. Roelant, 1996, Detection of leaks in underground storage tanks using electrical resistance methods, Journal of Environmental and Engineering Geophysics, Vol. 1, no. 3, 189-203.

Ramirez, A., W. Daily, D. LaBrecque, E. Owen and D. Chesnut, 1993, Monitoring an Underground Steam Injection Process Using Electrical resistance Tomography, Water Resources Research, vol. 29, no. 1, pp 73-87.

Figures

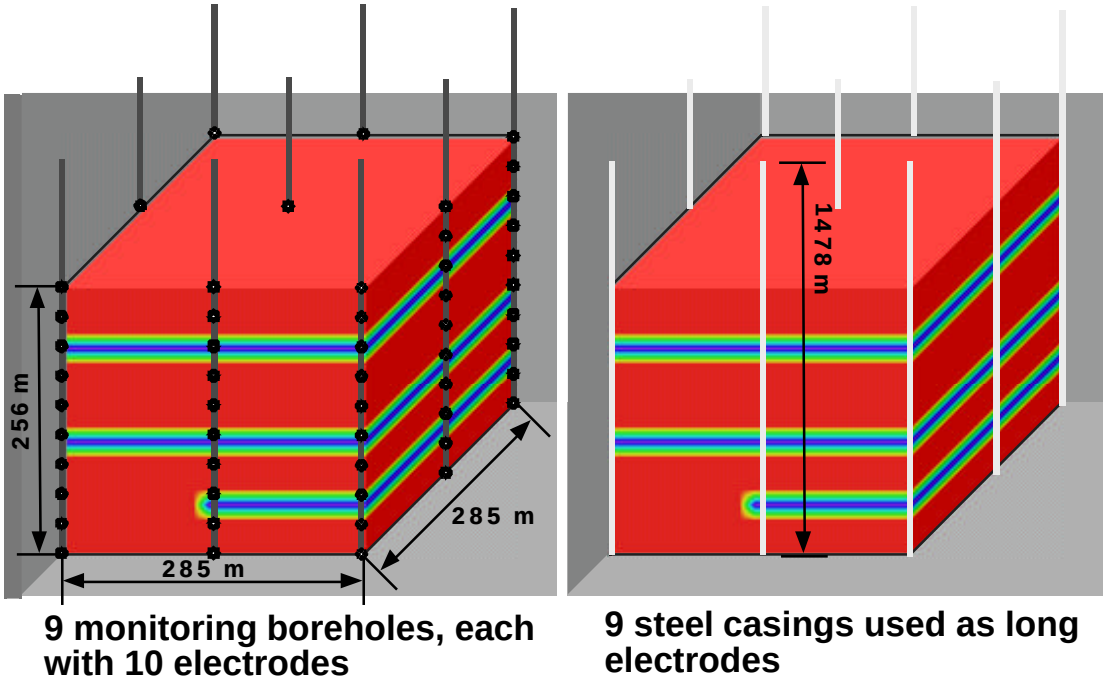

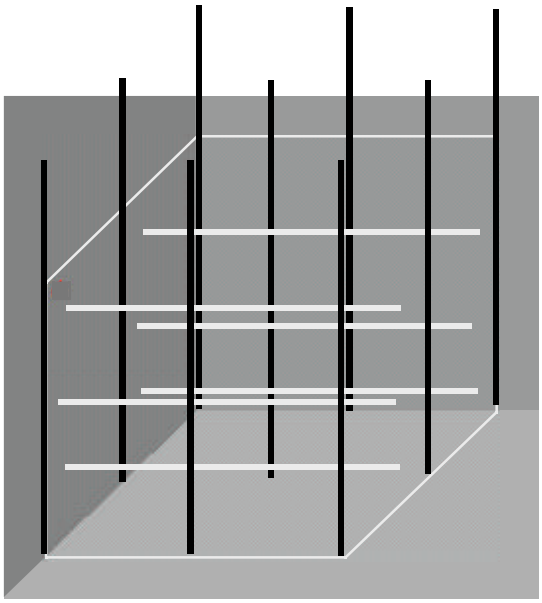

Figure 1. Electrode deployment scenarios considered by this study. Also shown is the resistivity model corresponding to the pre-flood or baseline case. The pre-flood resistivity of the layers was set to 10 ohm-m (purple layers) surrounded by a 100 ohm-m background (red layers).

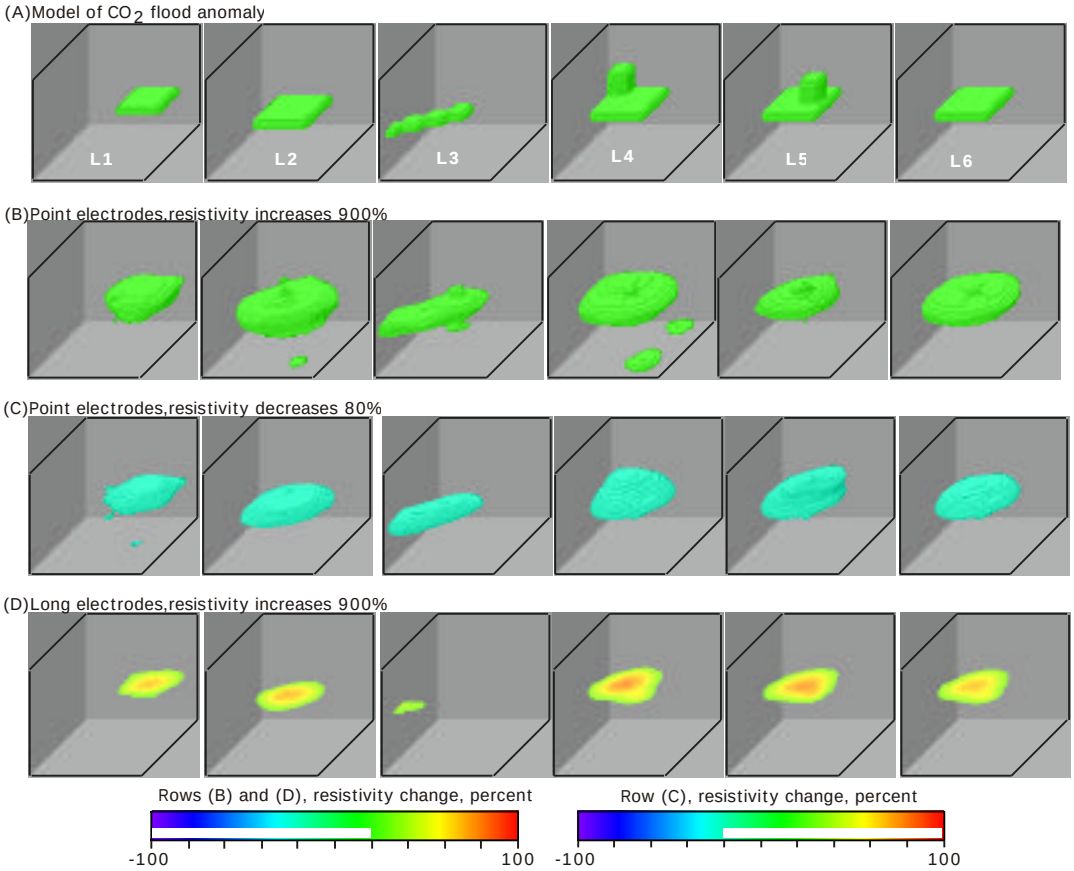

Figure 2. Results obtained for two electrode deployment scenarios: "point electrode" arrays and vertical casings used as long electrodes. The top row of images (row "A") shows the outline of the anomalies assumed. Rows "B" and "C" show some results for the "point" electrode simulations. Row "D" shows the results obtained when 9 vertical steel casings are used as very long electrodes. See text for discussion.

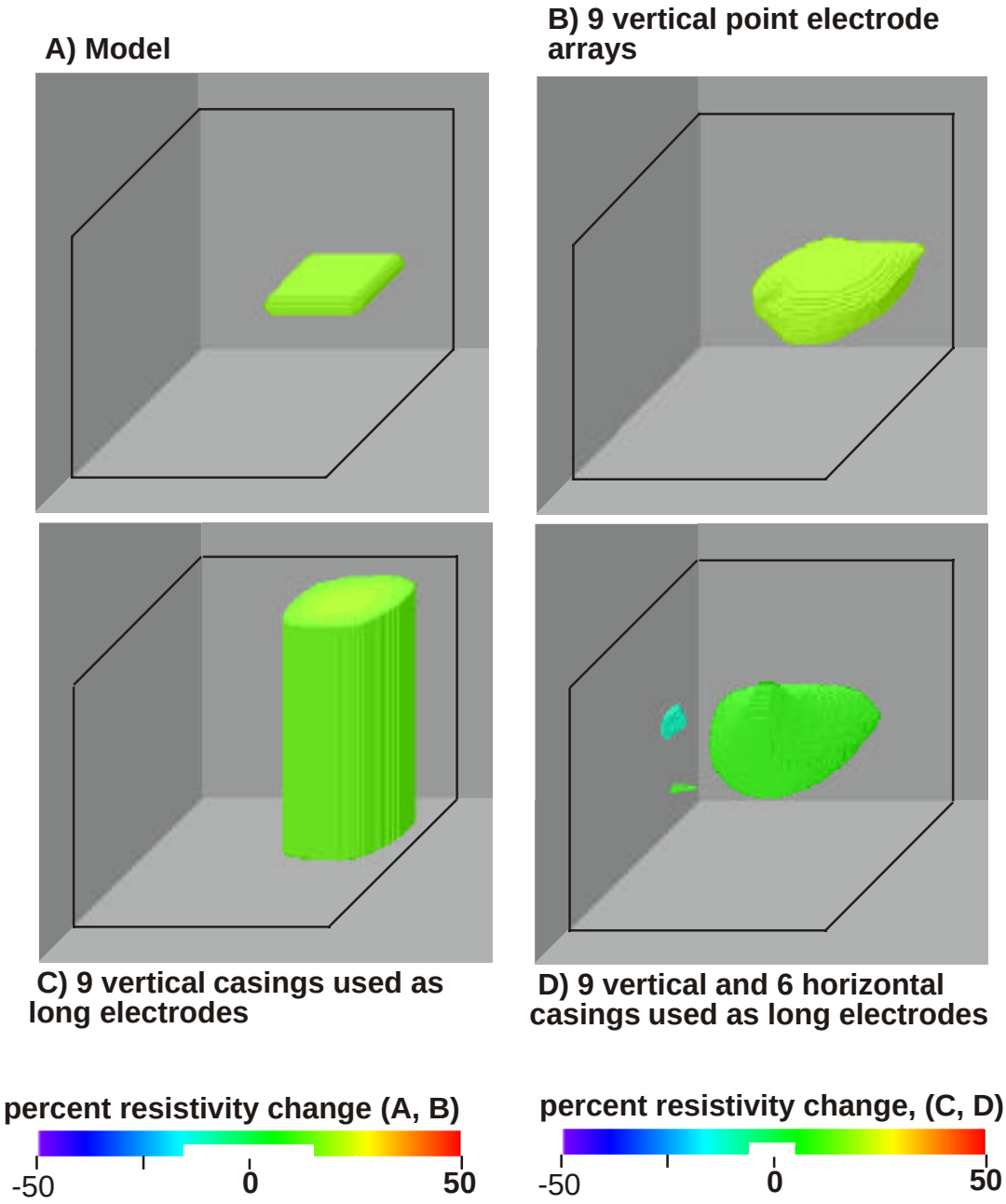

Figure 3. Results obtained using the three electrode deployment scenarios examined in this study. In this case, we compare the results for the L1 model when the center layer resistivity changes from 10 to 50 ohm-m.

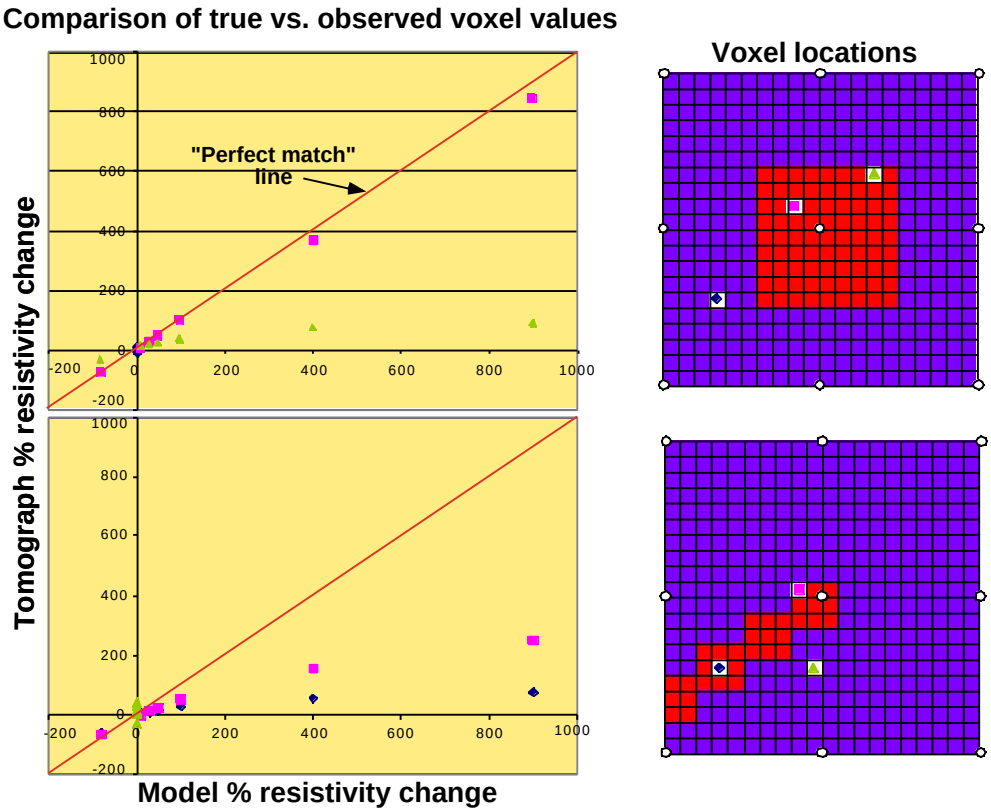

Figure 4. Influence of voxel position on the magnitude of the resistivity changes recovered by the tomographs. The graphs on the left side of Figure 4 compare the "true" percent resistivity change (in the model) to the recovered percent resistivity change in the tomograph for the various magnitudes of resistivity change considered. Horizontal slices through the 3D mesh are shown on the right hand side of the figure. These slices show the location of the anomalies in the mesh (orange color), the location of the point electrode arrays (white circles), and the location of the voxels to be examined in the graphs.

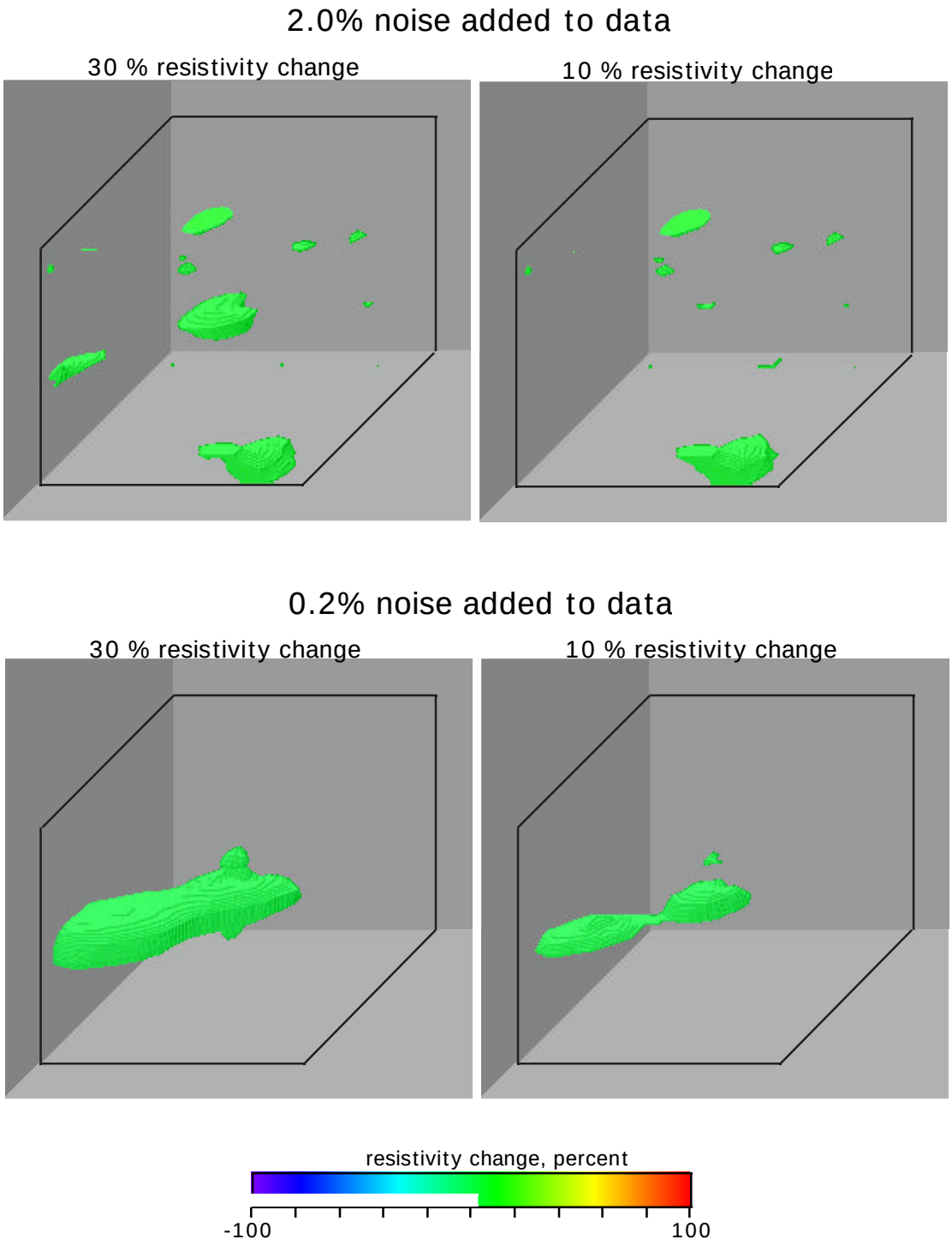

Figure 5. Results of simulations in which different levels of noise were added to the data. The top and bottom rows of images respectively show the results obtained when 2.0% and 0.2% noise were added to the data.

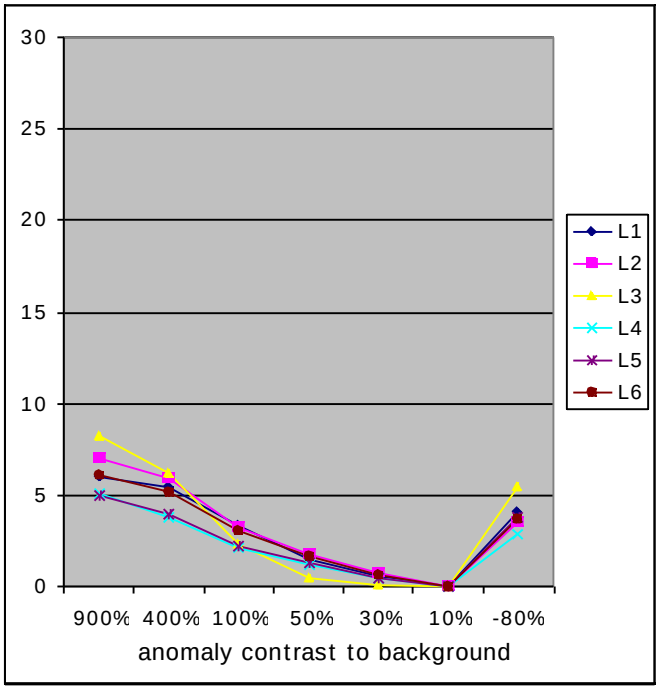

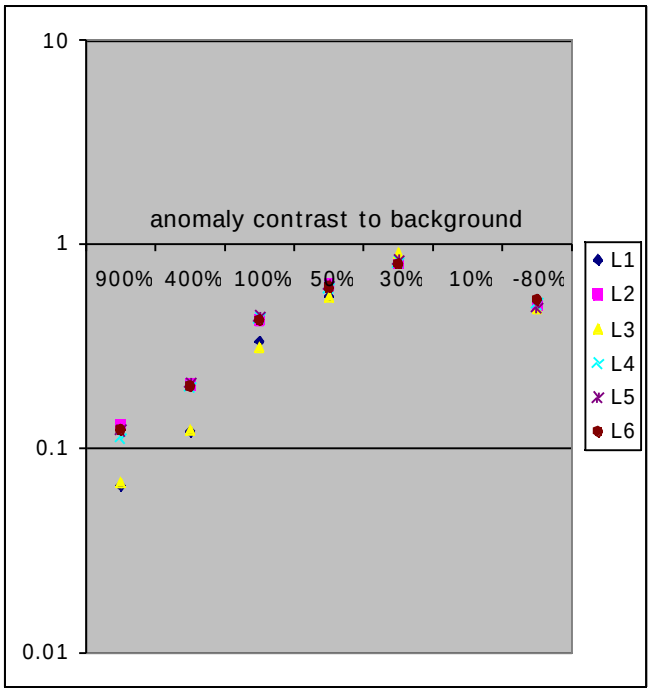

Figure 6. Comparison of the volume and average resistivity of the anomaly revealed by the tomographs and corresponding model values. The top graph shows the volume ratios obtained as a function of anomaly contrast and as function of model. The bottom compares the average tomograph resistivity of the voxels within the anomaly volume to the corresponding voxel resistivity values in the model.